RSC Advances

ROYAL SOCIETY
OF CHEMISTRY

www.rsc.org/advances

Size dependent catalytic activities of green synthesized gold nanoparticles and electro-

catalytic oxidation of catechol on gold nanoparticles modified electrode

Aftab Ahmad [a], Yun Wei [a], Fatima Syed [b], Muhammad Imran [b], Zia Ul Haq Khan [a], Kamran Tahir [a], Arif Ullah Khan [a], Muslim Raza [a], Qudratullah Khan [a] and Qipeng Yuan [a*]

[a] State Key Laboratory of Chemical Resource Engineering, Beijing University of Chemical Technology, No. 15 East Road of North Third Ring, Chao Yang District, Beijing 100029, China
[b] Institute of Chemical Sciences, Biochemistry Section, University of Peshawar - Peshawar 25120, KP, Pakistan

*Authors to whom correspondence should be addressed;

yuanqp@mail.buct.edu.cn,   aftabbiochem@yahoo.com

 Ph: +86 10 64437610, Fax: +86 10 64437610

Abstract

A green and facile method for the synthesis of gold nanoparticles (AuNPs) was developed. Phytochemicals from the aqueous extract of *Fagonia indica* were used to reduce and stabilize gold precursor (HAuCl$_4$) into gold nanoparticles. Various analytical techniques were used to determine size, morphology, composition, crystallinity, and capping biomolecules of the prepared gold nanoparticles. The appearance of characteristic surface plasmon resonance peak (SPR) at 542-565 nm revealed the synthesis of AuNPs (UV-Vis spectroscopy). XRD and EDX studies confirmed the face centered cubic structure and elemental composition of the green synthesized gold nanoparticles. Average particle sizes of 50, 20, and 70 nm were obtained by using the plant concentrations of 5, 10, and 15 mL respectively, with a fixed amount of HAuCl$_4$ (2 mM). The effect of synthesis variables (amount of plant extract and HAuCl$_4$) on the gold nanoparticles was also studied. Under the optimized conditions (10 mL plant extract + 2 mM HAuCl$_4$ and pH 8) the biogenic gold nanoparticles were well dispersed, small sized (15-20 nm), and mostly hexagonal in shapes. These *Fagonia indica* mediated Au-nanoparticles were observed to have strong catalytic activity for the photocatalytic reduction of methylene blue and chemical reduction of 4-nitrophenol. 80 % of MB could be photodegraded under visible-light irradiation after 80 min, showing the excellent photocatalytic activity of biogenic gold nanoparticles. Moreover, the catalytic activity was found to be size dependent. Cyclic votammetry (CV) indicated the electrochemical reversible oxidation of catechol at the green synthesized Au-NPs modified glassy carbon electrode. The Au-NPs modified electrode showed excellent catalytic activity with strong stability toward the electrochemical oxidation of catechol.

Keywords: *Fagonia indica*, Phytosynthesis, gold nanoparticles, photo and chemo-catalytic activities, electrochemical study

1. Introduction

Noble metal nanoparticles have attracted significant attention in the recent past due to their unique physiochemical characteristics, small size and enhanced optical properties. These nanostructure have a variety of applications in electronics, photo-chemistry, sensing, catalysis, medicines and energy storage devices [1, 2]. Noble metal nanoparticles can be effectively used as catalysts with efficient reactivity and excellent selectivity [3]. The improvement in catalytic activity, selectivity and the reduction in price of nanocatalysts would benefit chemical industry enormously. The catalytic potential of these nanoparticles have been exploited in the field of hydrogenation, carbonylation and hydroformylation etc. [4-6]. It has been well established that noble metal nanoparticles have the ability to absorb visible-light via surface plasmon resonance (SPR) that in turn enhances the photocatalytic reactivity [7, 8].

Several organic dyes are used in printing, paper and textile industries and a major portion of these dyes are lost and released into waters. Most of the organic dyes are non-biodegradable, circulate in water samples, and pose an environmental threat. Among the organic pollutants, nitro-aromatic compounds are considered as potential carcinogenic agents which are widely used for the fabrication of dyes, explosives, pharmaceuticals, and pesticides [9]. Furthermore, catechol and other dihydroxy benzene isomers are also toxic pollutants due to their low degradability and environmental toxicity [10]. These dihydroxy benzene derivatives are used in cosmetics, dyes, pesticides, and pharmaceutical industries [11]. Hence, there is clear need to detoxify these organic pollutants in environmental samples. The United States Environmental Protection Agency has declared nitrobenzene as one of the major toxic pollutants [12]. Therefore, it is highly imperative to mineralize organic pollutants in aqueous solutions using photocatalysts that utilize energy from the sunlight. TiO_2 is the most intensively studied photocatalyst. However, due to large band gap of TiO2, it can only utilize the UV light (4% of total light), resulting in low utilization of the

sunlight. A need exist to synthesize a photo-catalyst that could effectively utilize the visible light that account for 43% of the total sunlight.

The catalytic activity of noble metal nanoparticles are size, shape, and degree of dispersion dependent, as they control the surface structure, electronic and oxidation states. As compared to their bulk counterparts, metal particles at nanoscale often have significant catalytic properties that arise due to their increased surface-to-volume ratios and chemical behavior. Previous studies have demonstrated that smaller nanoparticles with spherical shapes are biologically more active than their larger counterparts [13]. Using single-molecule microscopy of fluorogenic reactions, X zhou *et al* demonstrated that the catalytic activity of gold nanoparticles are strongly dependent on their size [14]. The use of nanoscale material as a catalyst faces the intrinsic property of aggregation, which could lead to the ultimate loss of catalytic efficiency in practical applications. In order to cope with this problem, we optimized the synthesis protocol for preparation of well-dispersed and small size nanocatalyst that showed efficient catalytic performance.

Several physical and chemical methods have been used to synthesize metal nanoparticles [15-17]; however, all those methods are associated with several shortcomings such as the use of toxic chemicals and intensive energy and capital consumption. Greener approach of nanoparticles preparation is simple, cost effective and results in more stable nano-material. Among the green sources, plants appear to be the best candidates for large-scale production of nanoparticles with various shapes and sizes. The biomolecules present in plants can be used to reduce and stabilize metal ions in metal nanoparticles in a single-step green synthesis process. The use of biomolecules as a renewable source for the synthesis of metal nanoparticles in the ambient pressures and temperatures satisfies many aspects of green chemistry. Aqueous extracts of many

plants have been successfully used as reducing and capping agents for the green synthesis of metal nanoparticles.

In the current project, we synthesized well-dispersed gold nanoparticles using the aqueous extract of *Fagonia indica*. Furthermore, the effect of the synthesis variables (extract amount and $HAuCl_4$ concentrations) on the nanoparticles was also studied. The synthesized gold nanoparticles were evaluated for the photocatalytic degradation of methylene blue (MB) and chemical reduction of 4-nitrophenol in a size dependent manner. The green synthesized gold nanoparticles were also evaluated for the electrochemical oxidation of catechol (model reaction). This is the first report on using *Fagonia indica* for the phytosynthesis of gold metal nanoparticles and is among the few reports that describe the electrochemical properties of gold nanoparticles modified electrode.

2. Materials and method

2.1. Preparation of plant extract

Powdered plant material was washed several times with distilled water to remove any dust particles. A weighed amount (20 g) of the dust free plant was extracted in 250 mL de-ionized distilled water at 60 ºC for 30 min. The suspension was then stirred for 1 h at room temperature (24 ºC). This was followed by centrifugation at 5000 rpm for 10 minutes, and the supernatant was then filtered using filter paper (Whatman No.1). The clear filtrate obtained was used as a reducing and stabilizing agent for the synthesis of gold nanoparticles.

2.2. Synthesis of gold nanoparticles

For synthesis of gold nanoparticles (AuNPs,) varying amounts (5, 10 and 15 mL) of *fagonia indica* aqueous extract were added separately to the 30 ml of 2 mM aqueous gold solution ($HAuCl_4.4HO$). The reaction mixture was heated at 30 ºC (under vigorous stirring) and the formation of nanoparticles was observed from the visual observation of the color change from

pale yellow to violet. The progress of nanoparticles synthesis was monitored by UV-Vis spectroscopy. After 30 min of reaction, the colloidal suspension was centrifuged at 10,000 rpm for 10 min and the pellet obtained was washed thrice with distilled water and finally dried under vacuum.

2.3. Optimization of process parameters

Different concentrations (1-3 mM) of $HAuCl_4$. $4H_20$ was prepared for the synthesis of gold nanoparticles. *Fagonia indica* plant extract at varying concentration from 5 to 15 mL was added to gold solution and incubated at 30 ºC for 30 min. Reduction of gold ions into metallic nanoparticles of small size was optimized by varying the concentration plant extract and metal ions.

2.4. Characterization of nanoparticles

The prepared nanoparticles were characterized by various analytical techniques. UV-Vis spectroscopy was used to detect the appearance of surface plasmon resonance (SPR) peak of gold nanoparticles. Particle size and morphology were determined by high-resolution transmission electron microscopy (HRTEM). Dynamic light scattering technique (DLS) was used to determine the size distribution of gold nanoparticles capped by phytochemicals and their stability by zeta potential values. XRD and EDX studies were performed to determine the crystalline nature and elemental composition of the prepared nanoparticles respectively. The biomolecules that are involved in metal reduction and capping were investigated by FTIR spectroscopy. Thermogravimetric analysis (TGA) of phytosynthesized Au NPs was carried out in the temperature range of 40 Cº to 800 ºC on a Shimadzu DTG-60 thermal analyzer in nitrogen atmosphere. The heating rate was 10 ºC min^{-1}.

2.5. Photocatalytic activity

The photocatalytic activity of gold nanoparticles was evaluated by the reduction of methylene blue (MB) under visible light. Prior to irradiation, the suspension was magnetically stirred in dark for about 30 min to reach absorption-desorption equilibrium. The reaction was carried out in a mixture containing 20 mL MB solution (10 mg /L) and 10 mg of the powdered photo-catalyst of different sizes. During the photocatalytic reaction, the mixture containing methylene blue and photo-catalyst was magnetically stirred under visible light. At certain time intervals, 3 mL suspension was sampled and centrifuged (10,000 rpm) to remove the catalyst. The degradation of MB was monitored by a Shimadzu 2450 UV-vis spectrophotometer at 664 nm. The percentage degradation was calculated by following the equation,

$$Degradation \% = (\frac{Ac - At}{Ac}) \times 100$$

Where A_c is the absorbance of blank (control) (only dye solution exposed to visible light) and A_t is the absorbance of test (dye solution contains AuNPs exposed to visible light). A blank (dye solution without AuNPs) test was also run parallel to this experiment in order to evaluate the self-degradation of dye under visible light. The photocatalytic effect of AuNPs was calculated by subtracting from self-degradation of methylene blue under visible light.

2.6. **Catalytic reduction of 4-nitrophenol**

The reduction of 4-nitrophenol to 4-amino phenol was carried out in a quartz cuvette in the presence of 10 mg gold nanoparticles and 1 mL of aqueous 4-nitrophenol solution (1 mM) without stirring. Sodium borohydride (NaBH$_4$, 1.5 mL, 10 mM) was added which resulted in the color change from colorless to bright yellow. The change in color with time was quantitatively monitored using UV-visible spectroscopy. Time difference between the absorption measurements were 2 min.

2.7. **Electrodes preparation**

The GC electrode was polished with 1, 0.3 and 0.05 μm α-alumina powder respectively and then washed ultrasonically in methanol. For the preparation of AuNPs/GCE, the polished GC electrode was immersed in methanol suspension containing 5 mg each of AuNPs and activated charcoal, followed by evaporating the solvent at room temperature. The prepared AuNPs modified GC electrode was rinsed with distilled water to remove the loosely bound AuNPs. This modified electrode was used for subsequent experiments.

2.8. Votammetry

Electrochemical measurements were performed with electrochemical workstation (CH Instruments, Chenhua Co., Shanghai, China). A conventional three-electrode system was used in the measurements, with bare GCE or modified GCE as the working electrode, a Pt wire as the counter electrode and a saturated calomel electrode (SCE) as a reference electrode.

3. Results and discussion

3.1. UV-Vis spectroscopy

Formation of gold nanoparticles was confirmed from UV-visible spectral analysis. UV-Vis spectroscopy is a valuable technique to detect the characteristic SPR pattern of metal nanoparticles. Metal nanoparticles exhibit SPR phenomenon, where metal electrons in the conduction band collectively oscillate in resonance with certain wavelength of the incident light. The SPR pattern of metal nanoparticles depends on particle size, shape and the reaction medium [18]. Fig. 1 shows the time dependent evolution of UV-Vis spectra of aqueous solutions of gold nanoparticles prepared at varying amount of plant extract (5, 10 and 15 mL) and gold precursor (1, 2 and 3 mM $HAuCl_4$). The position and intensities of the SPR peaks varied with the concentration of plant extract and gold precursor ($HAuCl_4$). Fig. 1 a represents the effect of plant extract on the synthesis of gold nanoparticles using 1 mM $HAuCl_4$ solution. AuNPs revealed an

SPR band at 565 nm when 5 mL of the plant extract was mixed with 30 mL (1 mM) gold precursor. A low intensity of absorbance was observed at this concentration of plant extract, indicating the synthesis of small amount of nanoparticles. However, when 10 mL of the plant extract was used, the SPR peak blue shifted from 565 to 542 nm with the corresponding increase in peak intensity. This combine phenomenon indicates an increase rate of gold reduction into gold nanoparticles of small size particles distribution. The use of higher concentration of plant extract (10 mL) introduce more reducing and stabilizing agents, which favors gold reduction into stable gold nanoparticles. A further increase in the plant concentration (15 mL) resulted in a red shift and broadening of the SPR pattern, suggesting a possible increase in the particle size. Such an observation is expected due to an additional interaction among the AuNPs surface capping molecules and the secondary reduction process on the surface of preformed nuclei [19]. The observed increase in particle size at higher plant concentration may also be due to the elevated level of poly-phenolic contents. These compounds play a critical role in the formation of nanoparticles as has been previously reported for other plants [20].

Fig. 1 b-d represents the effect of plant extract on the synthesis of gold nanoparticles using 2 mM gold solution. Results indicated that maximum SPR intensity with narrow size particles distribution can be achieved at 10 mL plant extract and 2 mM gold solution (Fig. 1 c). Following the mixing of 10 mL plant extract with 2 mM $HAuCl_4$ solution, a change in color was observed within 2 min of the reaction, which is quite faster than most of the bio-based reports [21-23]. However, the SPR peaks red shifted above and below the optimum level (10 mL) of plant extract, indicating the probability of increasing particles size (Fig.1 b, d). In addition, the particle size was also controlled by varying the concentration of gold ions (keeping extract 10 mL). Fig. 1.e shows the UV-Vis spectrum of gold nanoparticles synthesized at 3 mM $HAuCl_4$ and 10 mL

plant extract. It was observed that the SPR peaks shifted from shorter to longer wavelength with the increasing concentration of $HAuCl_4$ solutions. The broad peak at 568 nm indicated that the prepared gold nanoparticles were polydispersed in the solutions [23]. The increase in the salt concentration also resulted visible precipitation with corresponding decrease in absorbance. Our results indicated that better size control and maximum production of gold nanoparticles could be achieved at 2 mM $HAuCl_4$ and 10 mL plant aqueous extract. Subsequent optimizations of other parameters were carried out by keeping the plant and salt concentrations at their optimum levels. Fig.1 f represents the effect of pH on the biosynthesis of AuNPs. Results showed that pH of the reaction media have strong influence on the biosynthesis of gold nanoparticles. Alkaline pH (pH 8) favored the synthesis of nanoparticles as evident from the saturation of the SPR peak intensity (at 542 nm) after 30 min, indicating a significant reduction of gold ions into metallic nanoparticles. Previous study reveals that noble metal ions are efficiently reduced at higher pH [18]. This observation suggests that higher pH induces more nucleation and growth of metal nanoparticles, which may be due to the activation of the phytochemicals involved in their synthesis in alkaline conditions. Similar results were reported by Kajani *et* al who stated that alkaline pH is suitable for the synthesis of silver and gold nanoparticles [24].

3.2. XRD

XRD analysis was carried out to determine the crystal structure of the prepared gold nanoparticles. The XRD pattern of gold nanoparticles is shown in Fig. 2. Results indicated that four conspicuous Bragg reflection peaks appeared at positions 38.23°, 44.45°, 64.62°, 77.64° that could be indexed to (111), (200), (220), (311) lattice planes of face centered cubic gold respectively (JCPDS file 04-0784). As evident from the observed pattern, the most significant peak is centered at $2\theta = 38.175°$, which is originated from the face centered cubic silver [25]. This result clearly shows that the top crystal plane (basal plane) of the synthesized nanoparticles must

be the (111) plane. Because of its high atomic density, the (111) facet is considered to be the most reactive facet. Similar diffraction patterns have been previously reported for silver and gold nanoparticles using plant extract as reducing and capping agents [26]. XRD peaks for gold nanoparticles synthesized under varying amount of plant extract, showed that AuNPs prepared with 10 mL extract (small size) had broader peak pattern (Fig. 2 A) than their larger counterparts synthesized with 5 and 15 mL extract (Fig. 2 B, C). This result is also in agreement with the particle size determined by HRTEM. In addition, the average crystal size of these particles was determined from full width half-maximum (FWHM) of the diffraction peaks using Debye–Scherrer's Eq. (1) given bellow:

$$d = \frac{K\lambda}{\beta \cos\theta} \qquad 1$$

Where, k is the Scherrer's constant, λ is the wavelength of the X-ray, β and θ are the half width of the peak and half of the Bragg angle, respectively. The size (d) of gold nanoparticles for sample A, B and C were determined to be approximately 20, 50 and 70 nm respectively.

3.3. Energy dispersive X-ray (EDX)

The presence of elemental gold in the prepared nanoparticles was confirmed by the energy dispersive X-ray analysis. The EDX pattern of gold nanoparticles is shown in Fig. 3. The appearance of strong peak around 2 KeV confirmed the elemental gold as a major constituent along with low signals from C, O and Cu atoms [27]. The weak signals designated as C and Cl may be due to the biomolecules that cape the nanoparticles. The Cu signal in Fig. 3 arose from the Cu grid used for analysis.

3.4. Transmission Electron Microscopy (TEM)

The shape and size of the phyto-synthesized gold nanoparticles were determined by high-resolution transmission electron microscopy. Fig. 4 shows the TEM images of the gold

nanoparticles obtained using different concentrations (5, 10, and 15 mL) of plant extract. Fig. 4 a-c represents the TEM images of gold nanoparticles synthesized at 5, 10 and 15 mL plant extract using 1 mM HAuCl$_4$ respectively. It is obvious from the HRTEM image (Fig. 4 a) that AuNPs synthesized at low extract concentration (5 mL) were irregular/quasi shapes with an approximate particle size of 50 nm. HRTEM results also revealed a low yield of the gold nanoparticles prepared under 5 mL of plant extract and 1 mM gold ions (agreement with low SPR intensity). Low quantities of the plant extract reduce the gold ions, but do not protect most of the nanoparticles from aggregation because of the deficiency of phytochemicals to act as protecting agents [28]. Inadequate capping of the gold precursor results in aggregation among the growing nuclei, which leads to larger particles size. Furthermore, at low extract concentration, the decreased reaction rate causes a decrease in the rate of gold nuclei formation, and therefore, fewer stable nuclei are produced. If the number of nuclei formed is low, the resulting particles will be larger in size[29].

The gold nanoparticles obtained under the optimized conditions (2 mM gold and 10 mL extract) were hexagonal, spheroidal and pyramidal in shapes with an approximate particle size of 20 nm. Also the nanoparticles were observed to be well separated from each other indicating an excellent capping of the gold ions. Optimum level of plant extract (10 mL) introduced sufficient reducing and capping agents, which properly reduce and cape the metal ions into metal nanoparticles. The capping agents can stabilize the growing nuclei by preventing the possible aggregation among the particles. On the other hand, when the amount of plant extract was further increased (15 mL), the AuNPs obtained were comparatively larger in size and of mixed shapes with some degree of aggregation (Fig. 4 f). Such an increase in particles size is expected as the presence of more reducing agents (at higher concentrations of extract) results in an additional

interaction between the surface capping biomolecules and the secondary reduction process on the surface of preformed nuclei giving rise to bigger particles[5, 19]. R. Emmanuel *et al*. demonstrated that at fixed concentration of gold ions, the particle size decreases with the increase in extract amount, however, any further increase in the plant extract results in an increase in the size of prepared gold nanoparticles[28]. Similar results were also reported by Reddy *et al.* where they prepared small and well dispersed gold nanoparticles at higher plant extract (45% W/V) as compared to low extract amount (15% W/V) [23]. The effect of gold precursor was also evaluated on the synthesis and size of gold nanoparticles. The gold nanoparticles synthesized at 3 mM $HAuCl_4$ and 10 mL plant extract were larger in size (60-80 nm) than those obtained at 2 mM gold precursor. Previous study also reveals a possible increase in particle size with the increasing concentration of $HAuCl_4$ [23]. HRTEM images of AuNPs prepared under high concentration of gold ions (3 mM) also revealed some degree of fusion among the particles. Such a size variation with gold concentration is in agreement with the UV-Vis data (Fig. 1 e).

3.5. Particles size distribution and stability

The size distribution of biogenic gold nanoparticles (AuNPs) was determined using DLS particle size analyzer. The average particles size of the AuNPs synthesized at 5 mL plant extract was found to be 50 nm (Fig. 5 A). Though the size distribution ranged between 40 to 60 nm, maximum percentage of the nanoparticles was observed in the range of 45-55 nm. The size distribution histogram of gold nanoparticles obtained at 10 ml plant extract reveals that maximum percentage of particles are in the size range of 15-25 nm (Fig. 5 b. It was also observed that gold nanoparticles prepared at higher plant extract (15 mL) were larger in size with maximum percentage in the size range of 60-80 nm (Fig. 5 c). The results obtained from DLS measurements are in close agreement with the HRTEM study. However, the difference in sizes

as observed from HRTEM and DLS may be due to the fact that the particle size determined by DLS is augmented significantly by the hydrated capping agents and solvation effects. In addition, the variation in sizes determined by different methods may also be attributed to the fact that these methods rely on different physical principles and/or detection methods.

The stability of the prepared samples was determined using zeta potential measurements. The zeta potential of a sample is most often used as an indicator of dispersion stability. Zeta potential of the prepared gold nanoparticles is shown in figure 5 B. Biogenic gold nanoparticles displayed lower zeta potential value at lower extract quantity (5 mL) and higher zeta potential values at a higher quantity (10 mL). The zeta potential value gradually increased from - 41 mV to -47.6 mV for gold nanoparticles synthesized at 5 and 10 mL plant extract indicating an increase stability of the prepared nanoparticles. Large zeta potentials predict a more stable dispersion. The negative value of zeta potential shows that gold nanoparticles are capped with negatively charged moieties which induce repulsion among the particles (avoiding agglomeration) and thereby increasing the stability [30]. The electrostatic repulsive interaction between the negatively charged nanoparticles may prevent the possible aggregation of the AuNPs, which might be responsible for their long-term stability [31].

3.6. FTIR

The FTIR study was performed to detect the possible biomolecules present in the aqueous extract of *Fagonia indica*, which are responsible for the reduction and capping of gold ions. Fig. 6 shows the FTIR spectra of *Fagonia indica* aqueous extract and *Fagonia indica* mediated gold nanoparticles. The FTIR spectrum of *Fagonia* aqueous extract shows several major peaks at 3404, 2922, 1640, 1322 and 1060 cm^{-1} respectively. Among them, the intense peaks at 3404 and 1640 cm^{-1} are associated with O-H stretching vibration of hydroxyl group of phenols/alcohols

and C=O stretching vibration of carboxylic and carbonyl groups of flavonoids (amid I) respectively. The other three peaks at 2922, 1322 and 1060 cm $^{-1}$ could be attributed to the NH stretching vibration of amid II, C-O stretch and C-N stretching amine respectively [32]. The FTIR spectrum of *Fagonia indica* mediated gold nanoparticles revealed a decrease in the peak intensities, suggesting a possible involvement of those groups in the synthesis and stabilization of gold nanoparticles. The gold nanoparticles showed some degrees shift corresponding to the stretching vibration of O-H bond in phenolic compounds from 3404 to 3432 cm $^{-1}$, the stretching vibration of C=O bond in flavonoids from 1640 to 1628 cm $^{-1}$ and the NH stretching vibration of amid II from 2922 to 9221 cm $^{-1}$. These observations suggest that the prepared AuNPs might be stabilized by various functional groups present in the biomolecules of *Fagonia indica* aqueous extract such as flavonoids, saponins, and proteins. The hydroxyl groups in these biomolecules could participate in the gold bio-reduction.

Au (III) + 3R–0H → Au (0) + 3R=O + 3H^{+}

Possible mechanism of gold reduction in to gold nanoparticles

3.7. Thermal behavior

Thermal behavior of gold nanoparticles containing samples was investigated with TGA and results are shown in Fig. 7. The total weight loss observed was about 29.1 and 40.71 % for AuNPs prepared from 10 and 15 mL extract respectively. This result indicated that AuNPs prepared from high plant extract were capped with more phytochemicals as compared with those synthesized from low amount. The weight loss due to the thermal decomposition of the organic part allowed to calculate the extract/gold ratio which is in agreement with the effect of extract/gold ratio on the size of gold nanoparticles (TEM and DLS experiments).

3.8. Photocatalytic activity

Photocatalytic activity of gold nanoparticles was evaluated by the reduction of methylene blue

(MB) under visible light (model reaction). A blank experiment was also performed in the

absence of gold nanocatalyst. The characteristic absorption peak of methylene blue appears at 664

nm. Fig. 8 shows the change of methylene blue relative concentrations as a function of irradiation

time. Slight degradation of methylene blue was observed in the absence of the photocatalyst

(AuNPs) after 2 h under visible-light irradiation (Fig. 8b). This can be accounted for the

photosensitized capability of methylene blue molecules [33]. However, in the presence of gold

nanoparticles, there was a gradual decline in the peak intensity at 664 nm with a successive red

shift, indicating the reduction of this dye. The decrease in peak intensity at 664 nm indicates the

reduction of MB to a colorless product "leucomethylene blue".

The photocatalytic activity of gold nanoparticles was studied at pH range 5-10 and maximum

activity was observed at pH 8 (Fig. 9c). Previous study also reveals that basic media is suitable

for an efficient catalytic activity of metal nanoparticles [34]. In addition, a linear increase in

catalytic activity was observed with the increasing concentration of gold nanoparticles (Fig. 9b).

However, no significant increase in activity was observed beyond 15 mg of the catalyst,

suggesting that photocatalytic activity of AuNPs decreased at high catalyst concentration. This

may be due to the fact that higher concentration causes agglomeration among the gold

nanoparticles which results in an increase in the particle size leading to decrease in specific

surface area of the particles and surface active sites [35].

The size of nanoparticles plays an important role in their catalytic activities. The size dependent

catalytic activity of gold nanoparticles was studied and the result is shown in scheme II. For

simplicity, the tested nanoparticles of different sizes are represented as A, B, and C. Where **A**

shows the AuNPs synthesized from 5 mL plant extract and 2 mM HauCl$_4$ (50 nm), **B** represents

AuNPs synthesized from 10 mL extract and 2 mM $HAuCl_4$ (15-20 nm) and **C** shows the AuNPs prepared from 10 mL extract and 3 mM $HAuCl_4$ (70 nm). Fig. 8 c-e represents the catalytic activities of sample A, B and C. The catalytic activity of sample B was significantly higher than A and C as evident from the successive decrease in absorbance at 664 nm. Sample B exhibited 80 % degradation rate of methylene blue in 80 min. Under the same experimental conditions, 67 and 56 % of methylene blue was photo-degraded by the sample C and A respectively (Fig. 9). The enhanced catalytic activity of sample B may be attributed to their small size, large surface area and increase surface electron density [36, 37]. It is well known that the surface area of a photocatalyst significantly affect its catalytic activity [38]. With greater available surface area, the adsorbed dye molecules might be able to diffuse more rapidly at the surface of the photocatalyst, causing the photoreactions to carry on more easily.

In order to compare the catalytic activities of all the catalysts, we calculated the reaction rate constants for Au nanocatalysts by plotting the absorbance at 664 nm verses time. The catalytic reaction followed first order kinetics as indicated from the linear correlation between $\log (A_t/A_0)$ and reaction time. The reaction rate constants were calculated from the slope of the lines, which were found to be 0.017, 0.024, and 0.03 min^{-1} for Au- nanoparticles of large, medium, and small sizes respectively (Fig. 8 c- d). A comparative analysis of dye degradation between the present study and other investigations previously reported reveals that the catalysis reaction rate is either equivalent or improved in our present process compared to most of the reported literature data [34, 39 40].

Metal nanoparticles mediate the transfer of electron from donor (phytoextract) to the reactant (MB), promoting a fast rely system for catalysis. The catalytic activity of metal nanoparticles strongly depends on their reduction potential in the catalytic process. The nano forms of metals

are catalytically more active, as they have negative redox potential compared to their bulk forms
[41]. It is well known that noble metals adopt a negative potential in nano-crystalline form and are therefore, catalytically more active than their bulk masses [42]. For efficient catalytic activity, metal nanoparticles need to have a redox potential between those of donor and acceptor groups [43]. In such a system, the metal nanoparticles behave as mediator that transfer electron between the donor specie (phytoextract) and acceptor substrate (methylene blue). This kind of electron transfer phenomenon in which metal nanocrystals act as redox catalyst is known as electron relay effect. A possible mechanism of electron transfer from the surface of nanoparticles to the dye is given in scheme 1. The redox potential of metal nanoparticles proportionally increases with the increase of the particle size [44, 45]. For a known concentration of gold nanoparticles, the smaller the sizes of gold nanoparticles, the more negative be the potential of gold nanoparticles that makes a larger potential difference between gold and dyes and hence a higher catalytic activity [46].

3.9. Reduction of nitro phenol

The pollution caused by various organic species such as phenol and other nitro- aromatic compounds is of great public concern. Among the organic pollutants, nitrophenols and their derivatives are the most important pollutants that result from the production processes of pesticides, insecticides, herbicides, and synthetic dyes [5, 12]. Furthermore, there is a high demand of the aromatic amino compounds in industry; therefore, the catalytic reduction of nitro-phenol to aminophenol is an important reaction from both academic and technologically point of view.

Fig. 10 b illustrates the UV-Visible spectra for the reduction of 4-nitrophenol as a function of time. Though the reduction of 4-nitrophenol to 4-aminophenol using aqueous $NaBH_4$ is thermodynamically favorable (E_0 for 4-NP/4-AP = -0.76 V and H_3BO_3/BH_4^- = -1.33 V versus

NHE), however, the reaction is kinetically unfavorable due to large potential difference between donor and acceptor species. The reaction is catalyzed in the presence of metal nanoparticles, which facilitate the transfer of electrons from the donor (BH_4^-) to acceptor molecule (4-NP). The 4-nitrophenol exhibits maximum absorbance around 317 nm, which red shifts to around 400 nm in the presence of sodium borohydride. The red shift in the absorbance peak is attributed to the formation of an intermediate 4-nitrophenolate ion in the presence of $NaBH_4$. The progress of nitro-phenol reduction can be monitored by the successive decrease of absorbance at 400 nm. In the absence of gold nanoparticles, a slight decrease in absorbance was observed at 400 nm. However, in the presence of gold nanoparticles, there was a rapid decline in the absorbance intensity at 400 nm and a concomitant appearance of a new peak at 298 nm revealing the reduction of 4-nitrophenol to 4-amino phenol [5].

The effect of particles size on the catalytic reduction of nitrophenol was also investigated. Results indicated that the rate of reaction was faster in the presence of small size gold nanoparticles as compared to their larger counterparts. The data (Fig. 10 a) shows that the reaction terminates within 10 min in the presence of sample B (15-20 nm) gold nanoparticles. However, the rate of this reaction was significantly lower when carried out in the presence of large size gold nanoparticles (Fig. 10 e). Rate constants (K) were calculated from the slopes of the linear plots obtained from the ln (A_t/A_0) verses time. Here, A_t shows the absorbance at any time and A_0 stands for the absorbance at zero time. The highest K value was observed for the reaction catalyzed by particles of small size (k = 0.24 min^{-1}) and was found to decrease with the increasing particle size. As the catalytic reaction takes place on the surface of nanoparticles and particles with small size, provide large surface area for reactant adsorption and chemical reaction. Previous studies also suggest that rate of catalytic reduction of nitrophenol decreases

with the increase in particle size [5]. The catalytic efficiency of the prepared gold nanoparticles is significantly higher than most of the previously reported green synthesized gold nanoparticles [23, 47]. Thus, the Au- nanoparticles synthesized from the aqueous extract of *Fagonia indica* might be potent nanocatalyst for the industrial applications.

3.10. Electrochemical property of gold nanoparticles modified GC electrode

In order to assess the electrochemical behavior of catechol, the cyclic voltammograms were performed in the presence and absence of catechol at gold nanoparticles modified GC electrode. Fig. 11A and 11B show CV responses of glassy carbon electrode (GCE) and assembled AuNPs electrodes *vs* saturated calomel electrode (SCE) in the absence (a) and presence of catechol (b) in sodium acetate (0.15 M) as supporting electrolyte. Fig. 11A shows one anodic and one cathodic peak of equal intensity for the reversible oxidation of catechol (**1a**) to a highly reactive quinone (**2a**). The redox couple of IpA/IpC for this reaction is equal to unity, which can be considered as a criterion for the stability of o-benzoquinone produced at the surface of electrode under the experimental conditions [48].

The Au-nanoparticles modified electrode did not show any observable redox peak response in the absence of catechol (curve a), indicating that the gold nanoparticles modified electrode is electrochemically inert in sodium acetate. However, a sharp reversible oxidation peak along with a small peak was observed at 0.37 and 0.69 V in the presence of catechol, which is attributed to the direct oxidation of catechol to quinone with two-electron and proton process. The appearance of second oxidation peak indicates the oxidation of intermediate formed. On the reverse scan, a strong reduction peak was observed around -0.042 V, which is due to the reversible reduction of quinone to catechol. The co-appearance of anodic peak A and a corresponding cathodic peak C are attributed to the transformation of catechol to quinone and vice versa within a quasi-

reversible two proton, two-electron reaction [48]. In other words, any dimerization or hydroxylation reactions are too slow to be observed on the time scale of cyclic votammetry [49].

Fig.11 C represents the effect of scanning rate on redox couple of catechol. During the following successive scanning, the oxidation peaks positively shifted to 0.370 V (at 100 mV/s) while the corresponding reduction peaks negatively shifted to -0.04 V at the AuNPs modified electrode. These changes are probably due to the formation of a thin film of product at the surface of the electrode, inhibiting the electrode process to some extent [50]. These observations suggest that the AuNPs modified electrode can act as a promoter to enhance the electrochemical reaction. A linear correlation was observed between the anode and cathode peak currents and the square root of the scan rate ($v^{1/2}$). This linear relationship indicates that the electrode reaction of catechol on the silver and gold modified electrodes was a typical diffusion-controlled process [51]. Based on all these observations, a mechanism was proposed for the electrochemical oxidation of catechol in to o-quinone, a reactive specie, as shown in scheme III.

4. Conclusion

A green, simple, and effective method has been used for the synthesis of AuNPs using aqueous extract of *Fagonia indica*. The size of gold nanoparticles can be controllably varied (~20 nm to 70 nm) by changing the concentration of *Fagonia indica* aqueous extract. The EDX and XRD analyses confirmed the presence of pure phase Au-nanoparticles. The synthesis of gold nanoparticles and their surface adhered biomolecules were determined by UV-Visible and FTIR spectroscopy respectively. The catalytic activities of gold nanoparticles suggests that AuNPs from 10 mL plant extract and 2 mM of $HAuCl_4$ have better catalytic properties than those from 5 and 15 mL plant extract and 1 and 3 mM $HAuCl_4$. Results indicated that the catalytic rate constant for the reduction of MB and 4-Nitrophenol are dependent on the size of gold

nanoparticles. These studies further suggest that the phyto-synthesized Au- nanoparticles have strong capacity for future applications in catalysis. The AuNPs modified GC electrode exhibited significant electro-catalytic activity toward the reversible oxidation of catechol. Furthermore, AuNPs modified electrode could be effectively used to detoxify phenolic and other nitro-aromatic compounds in water samples.

Acknowledgments

References

1.   M.-C. Daniel and D. Astruc, *Chemical reviews*, 2004, **104**, 293-346.

2.   R. Jin, Y. C. Cao, E. Hao, G. S. Métraux, G. C. Schatz and C. A. Mirkin, *Nature*, 2003, **425**, 487-490.

3.   H. Xu, J. Xu, Z. Zhu, H. Liu and S. Liu, *Macromolecules*, 2006, **39**, 8451-8455.

4.   S. Schimpf, M. Lucas, C. Mohr, U. Rodemerck, A. Brückner, J. Radnik, H. Hofmeister and P. Claus, *Catalysis Today*, 2002, **72**, 63-78.

5.   A. Gangula, R. Podila, L. Karanam, C. Janardhana and A. M. Rao, *Langmuir*, 2011, **27**, 15268-15274.

6.   M. Zahmakıran and S. Özkar, *Nanoscale*, 2011, **3**, 3462-3481.

7.   X. Chen, H. Y. Zhu, J. C. Zhao, Z. F. Zheng and X. P. Gao, *Angewandte Chemie*, 2008, **120**, 5433-5436.

8.   X. Zhou, G. Liu, J. Yu and W. Fan, *J. Mater. Chem.*, 2012, **22**, 21337-21354.

9.   Y. Zhang, X. Bo, C. Luhana, H. Wang, M. Li and L. Guo, *RSC Advances*, 2013, **3**, 17300-17306.

10.   D.-M. Zhao, X.-H. Zhang, L.-J. Feng, L. Jia and S.-F. Wang, *colloids and surfaces B: Biointerfaces*, 2009, **74**, 317-321.

11.   J. Wang, J.-N. Park, X.-Y. Wei and C. W. Lee, *Chemical Communications*, 2003, 628-629.

12.   A. Zosel, K. Rychter and J. B. Leikin, *American journal of therapeutics*, 2007, **14**, 585-587.

13.   S. Agnihotri, S. Mukherji and S. Mukherji, *RSC Advances*, 2014, **4**, 3974-3983.

14.   X. Zhou, W. Xu, G. Liu, D. Panda and P. Chen, *Journal of the American Chemical Society*, 2009, **132**, 138-146.

15.   H. Ma, B. Yin, S. Wang, Y. Jiao, W. Pan, S. Huang, S. Chen and F. Meng, *Chemphyschem*, 2004, **5**, 68-75.

16.   K. Mallik, M. Mandal, N. Pradhan and T. Pal, *Nano Lett.*, 2001, **1**, 319-322.

17.   D. Wostek-Wojciechowska, J. K. Jeszka, P. Uznanski, C. Amiens, B. Chaudret and P. Lecante, *Materials Science-Poland*, 2004, **22**, 407-413.

18.   A. A. AbdelHamid, M. A. Al-Ghobashy, M. Fawzy, M. B. Mohamed and M. M. Abdel-Mottaleb, *ACS Sustainable Chemistry & Engineering*, 2013, **1**, 1520-1529.

19.   S. Link and M. A. El-Sayed, *The Journal of Physical Chemistry B*, 1999, **103**, 8410-8426.

20.   V. Kumar, S. C. Yadav and S. K. Yadav, *J. Chem. Technol. Biotechnol.*, 2010, **85**, 1301-1309.

21.   Y. Wang, X. He, K. Wang, X. Zhang and W. Tan, *Colloids and Surfaces B: Biointerfaces*, 2009, **73**, 75-79.

22.   R. Vijayakumar, V. Devi, K. Adavallan and D. Saranya, *Physica E: Low-Dimensional Systems and Nanostructures*, 2011, **44**, 665-671.

23.   V. Reddy, R. S. Torati, S. Oh and C. Kim, *Industrial & Engineering Chemistry Research*, 2012, **52**, 556-564.

24.   A. A. Kajani, A.-K. Bordbar, S. H. Z. Esfahani, A. R. Khosropour and A. Razmjou, *RSC Advances*, 2014, **4**, 61394-61403.

25.   P. D. D. Files, *Pennsylvania, PA*, 1991.

26.   M. Nasrollahzadeh, S. M. Sajadi, F. Babaei and M. Maham, *Journal of colloid and interface science*, 2015, **450**, 374-380.

27.   A. Ahmad, F. Syed, A. Shah, Z. Khan, K. Tahir, A. U. Khan and Q. Yuan, *RSC Advances*, 2015, **5**, 73793-73806.

28.   R. Emmanuel, C. Karuppiah, S.-M. Chen, S. Palanisamy, S. Padmavathy and P. Prakash, *Journal of hazardous materials*, 2014, **279**, 117-124.

29.   A. Panáček, L. Kvitek, R. Prucek, M. Kolar, R. Vecerova, N. Pizurova, V. K. Sharma, T. j. Nevečná and R. Zboril, *The Journal of Physical Chemistry B*, 2006, **110**, 16248-16253.

30.   A. K. Suresh, M. J. Doktycz, W. Wang, J. W. Moon, B. Gu, H. M. Meyer III, D. K. Hensley, S. T. Retterer, D. P. Allison and T. J. Phelps, *Monodispersed biocompatible Ag2S nanoparticles: Facile extracellular bio-fabrication using the gamma-proteobacterium, S. oneidensis*, Oak Ridge National Laboratory (ORNL); Center for Nanophase Materials Sciences; High Temperature Materials Laboratory, 2011.

31.   B. Salopek, D. Krasić and S. Filipović, *Rudarsko-geološko-naftni zbornik*, 1992, **4**, 147-151.

32.   B. H. Stuart, *Infrared spectroscopy: Fundamentals and applications*, 2004, 71-93.

33. F. Ji, C. Li and J. Zhang, *ACS applied materials & interfaces*, 2010, **2**, 1674-1678.

34. P. Kumari, P. Chandran and S. S. Khan, *Journal of Photochemistry and Photobiology B: Biology*, 2014, **141**, 235-240.

35. K. Tahir, S. Nazir, B. Li, A. U. Khan, Z. U. H. Khan, A. Ahmad and F. U. Khan, *Separation and Purification Technology*, 2015, **150**, 316-324.

36. Z. Wei, J. Sun, Y. Li, A. K. Datye and Y. Wang, *Chem. Soc. Rev.*, 2012, **41**, 7994-8008.

37. S. Tokonami, N. Morita, K. Takasaki and N. Toshima, *The Journal of Physical Chemistry C*, 2010, **114**, 10336-10341.

38. J. Li, J. Xu, W.-L. Dai, H. Li and K. Fan, *Applied Catalysis B: Environmental*, 2009, **85**, 162-170.

39. T. Sinha and M. Ahmaruzzaman, *Journal of colloid and interface science*, 2015, **453**, 115-131.

40. R. Tripathi, N. Kumar, A. Shrivastav, P. Singh and B. Shrivastav, *Journal of Molecular Catalysis B: Enzymatic*, 2013, **96**, 75-80.

41. B. Hvolbæk, T. V. Janssens, B. S. Clausen, H. Falsig, C. H. Christensen and J. K. Nørskov, *Nano Today*, 2007, **2**, 14-18.

42. M. Haruta, N. Yamada, T. Kobayashi and S. Iijima, *J. Catal.*, 1989, **115**, 301-309.

43. K. Mallick, M. Witcomb and M. Scurrell, *Materials chemistry and physics*, 2006, **97**, 283-287.

44. A. Henglein, *Chem. Rev.*, 1989, **89**, 1861-1873.

45. M. Mostafavi, J. Marignier, J. Amblard and J. Belloni, *International Journal of Radiation Applications and Instrumentation. Part C. Radiation Physics and Chemistry*, 1989, **34**, 605-617.

26

46.   A. J. Bard and L. R. Faulkner, *Electrochemical methods: fundamentals and applications*, Wiley New York, 1980.

47.   I. K. Sen, K. Maity and S. S. Islam, *Carbohydrate polymers*, 2013, **91**, 518-528.

48.   M. R. Deakin, P. M. Kovach, K. Stutts and R. M. Wightman, *Analytical chemistry*, 1986, **58**, 1474-1480.

49.   H. Jaegfeldt, T. Kuwana and G. Johansson, *Journal of the American Chemical Society*, 1983, **105**, 1805-1814.

50.   H. L. Z. Zhad, M. Banitaba, M. A. Roozbahani and S. H. Davarani, *ECS Electrochemistry Letters*, 2012, **1**, G4-G6.

51.   W. Xiong, M. Wu, L. Zhou and S. Liu, *RSC Advances*, 2014, **4**, 32092-32099.
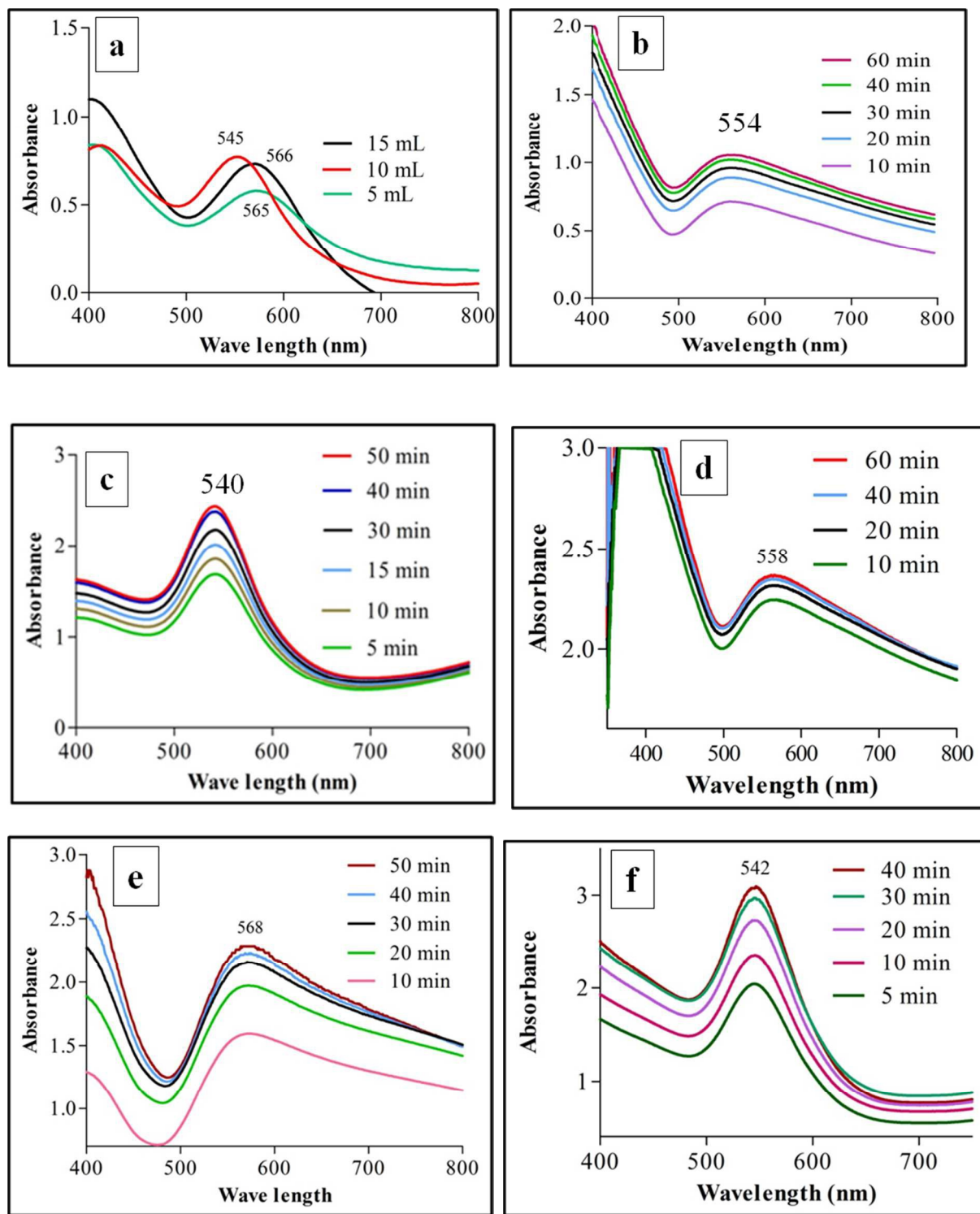
Fig. 1. UV-Vis spectra of green synthesized gold nanoparticles (a). Effect of the plant concentration (5, 10, 15 mL) on the SPR pattern of gold nanoparticles using 1 mM HAuCl4, (b-d), time dependent evolution of UV-Vis spectra of AuNPs using 5, 10 and 15 mL plant extract and 2 mM gold precursor, (e) synthesis of AuNPs using 10 mL extract and 3 mM HAuCl4, (f) AuNPs under the optimized conditions (10 mL extract, 2 mM HAuCl4 and pH 8)
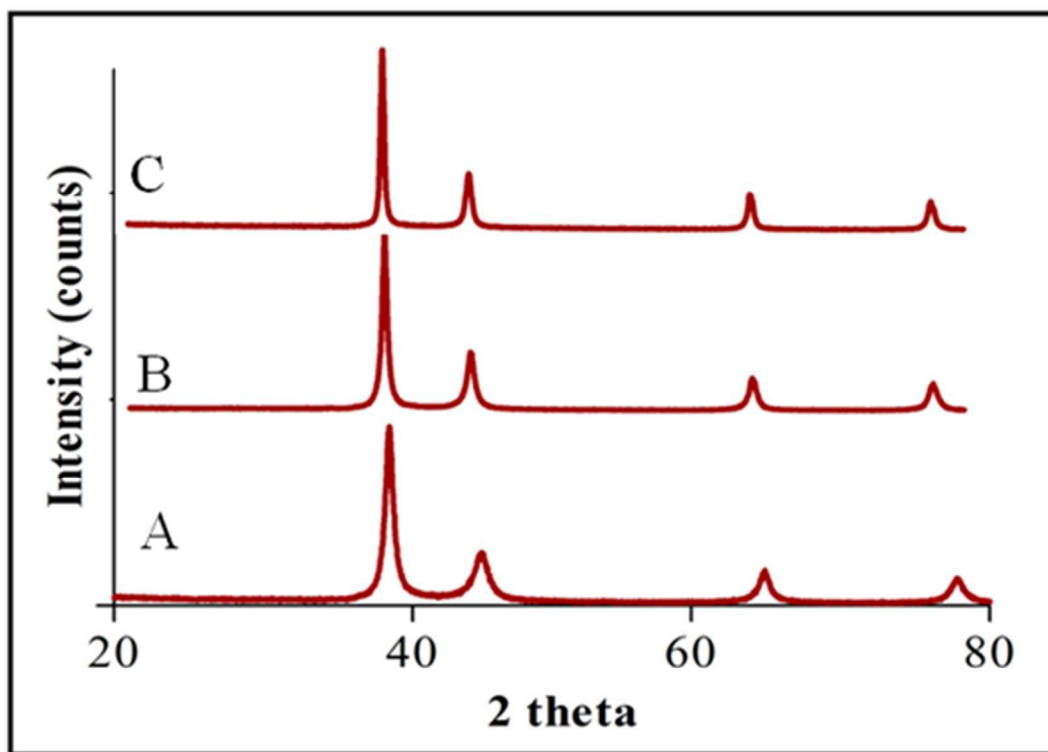
Fig. 2. XRD pattern of green synthesized gold nanoparticles using (A) 10 mL (B) 5 mL and (C) 15 mL of plant extract with a fixed amount of HAuCl$_4$ (2 mM)
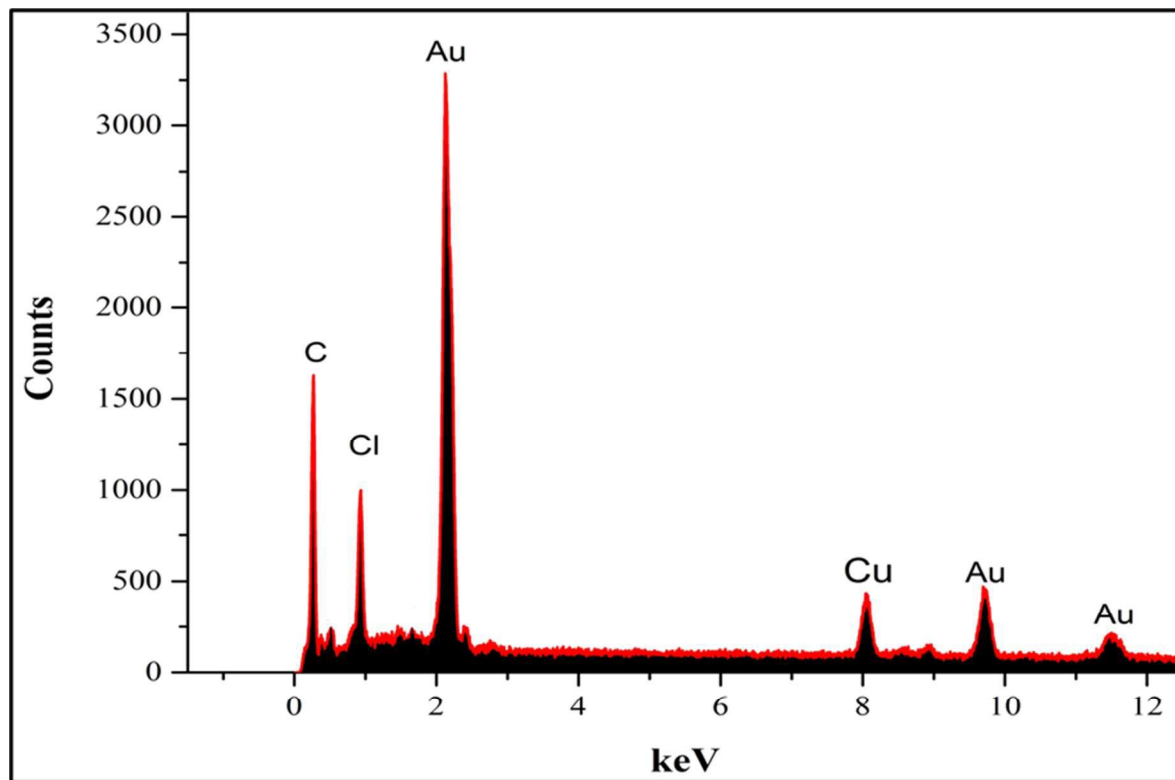
Fig. 3. EDX profile of *Rhazya stricta decne* mediated synthesized gold nanoparticles
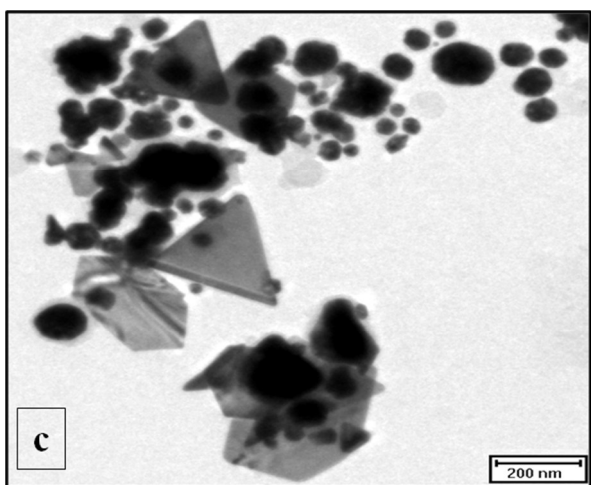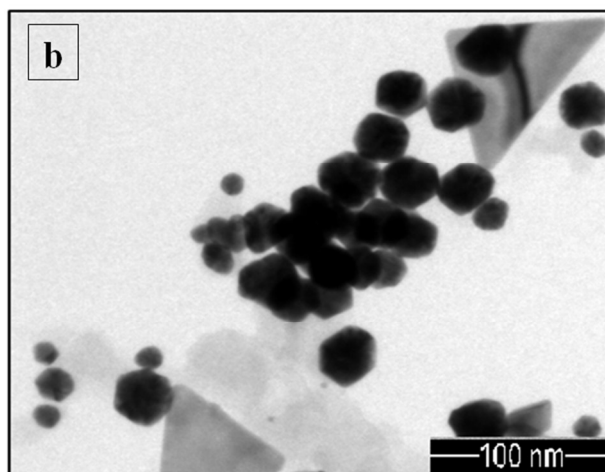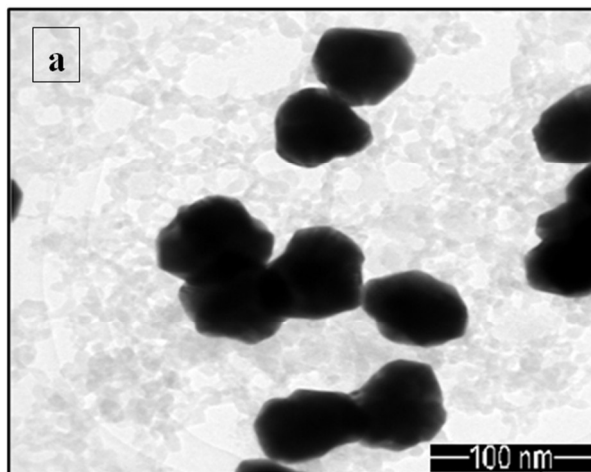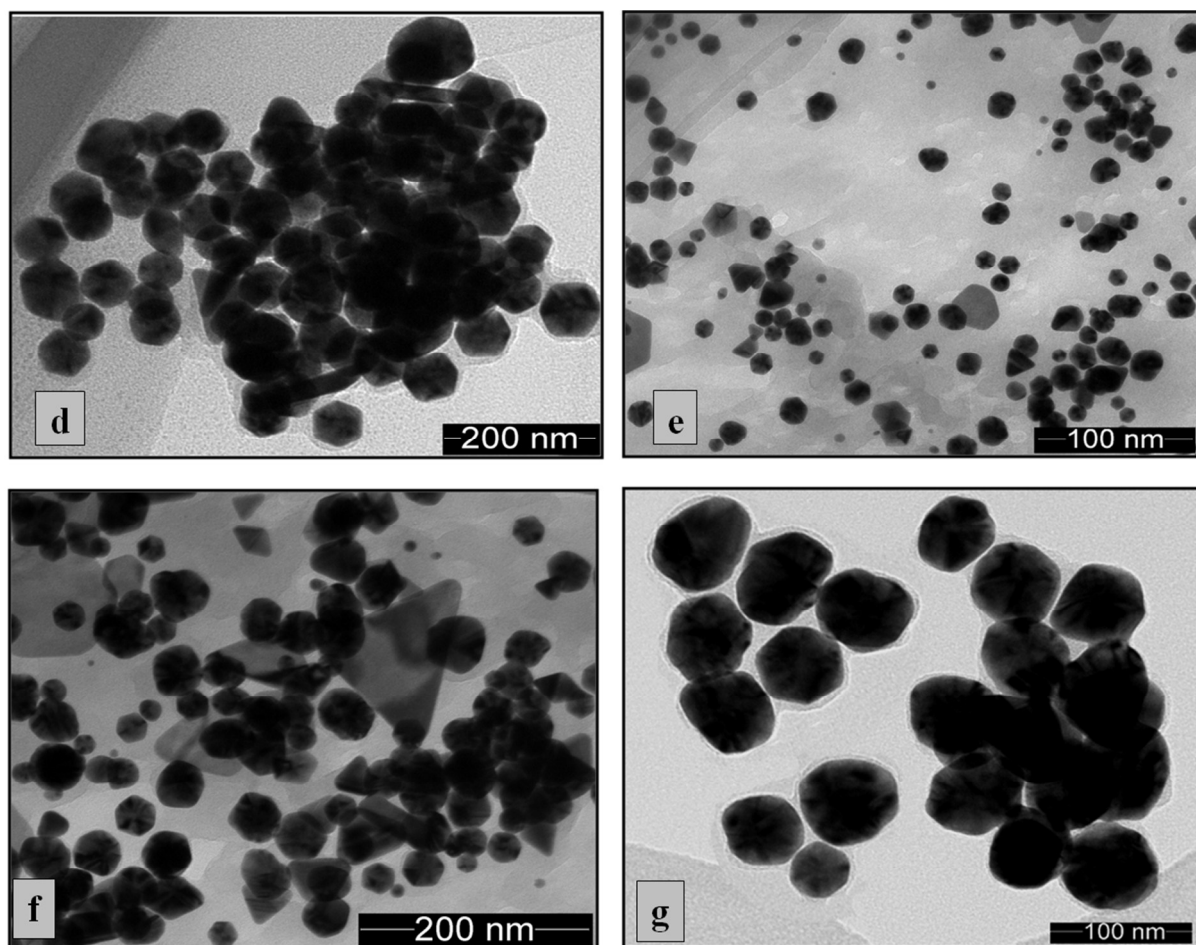
Fig. 4. HRTEM images of biogenic gold nanoparticles synthesized under varying amount of plant extract and gold precursor. (a-c) gold nanoparticles synthesized using 5, 10 and 15 mL plant extract and 1 mM $HAuCl_4$ respectively. (d-f) AuNPs using 5, 10 and 15 mL extract and 2 mM $HAuCl_4$ respectively. (g) showing gold nanoparticles prepared with 10 mL extract and 3 mM $HAuCl_4$
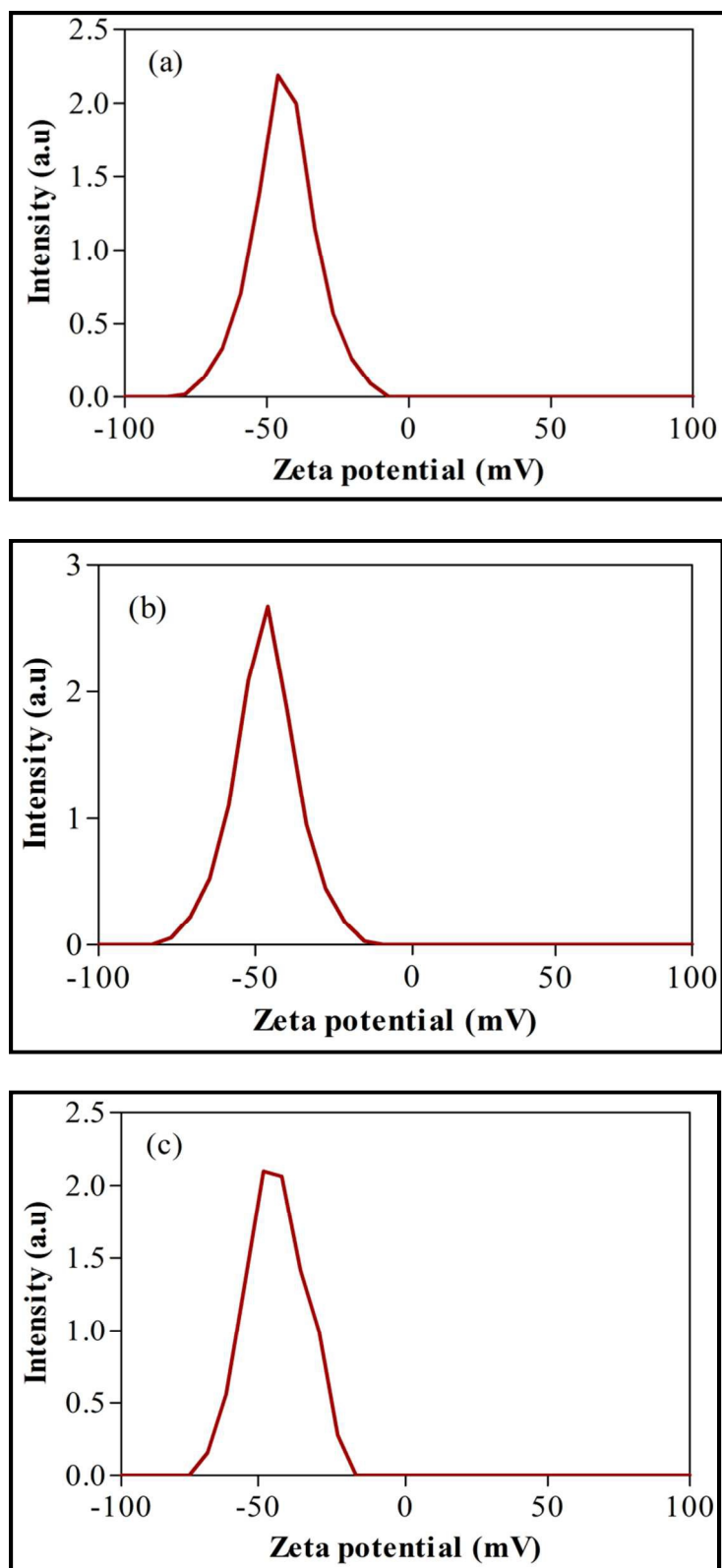
Figure 5 A. Zeta potential of AuNPs synthesized at (a) 5 mL (b) 10 mL and (c) 15 mL aqueous extract of *fagonia indica* and 2 mM HAuCl$_4$. 4H$_2$O
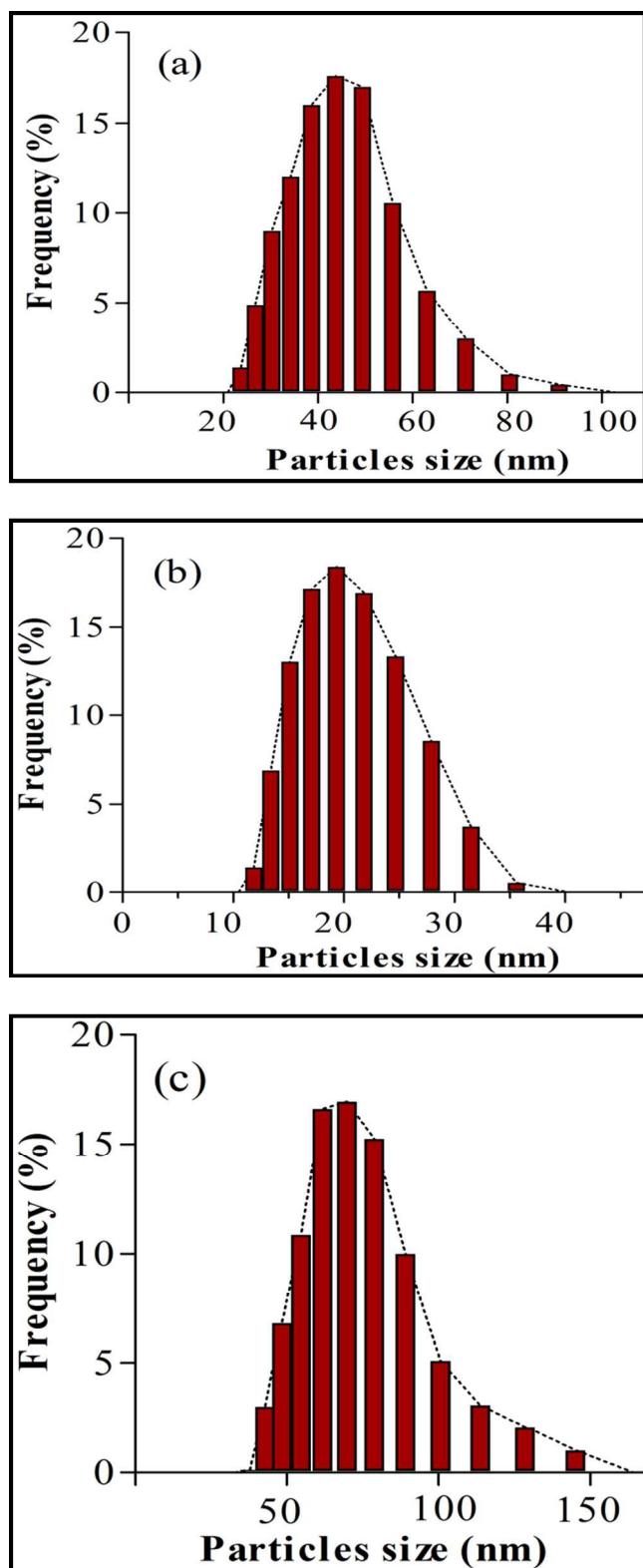
Figure 5 B. Size distribution of AuNPs synthesized at (a) 5 mL (b) 10 mL and (c) 15 mL aqeious extract and 2 mM HAuCl$_4$. 4H$_2$O

Figure 6
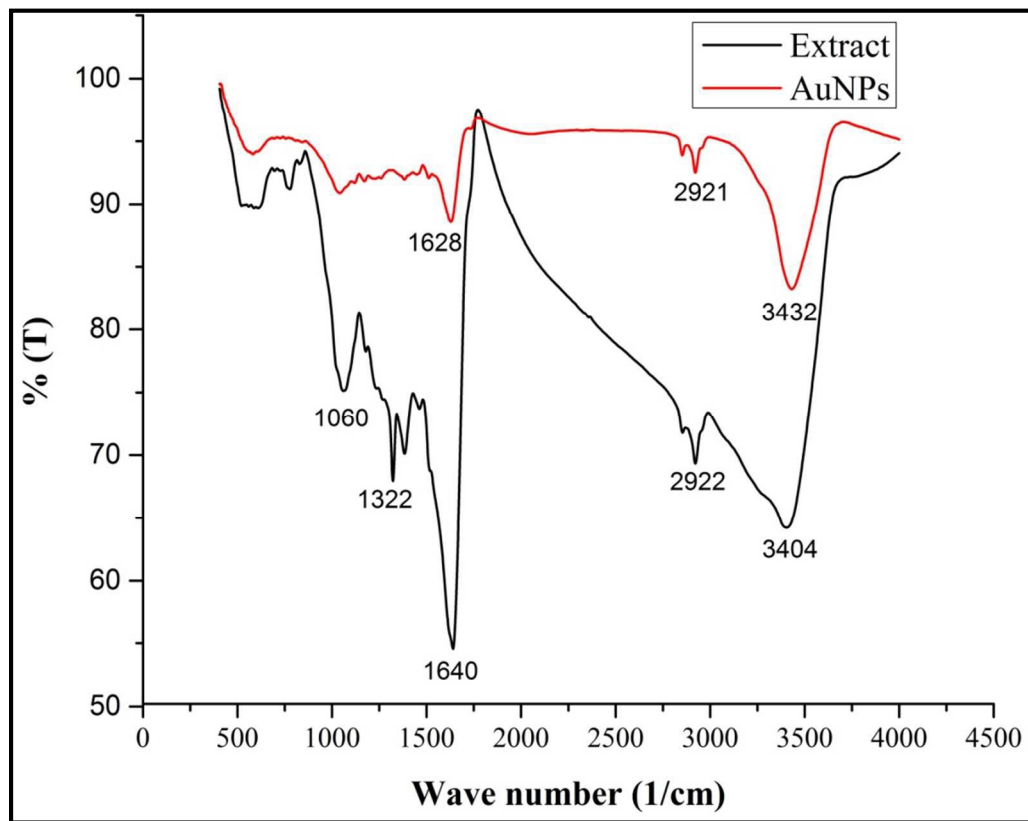
Fig. 6. FT-IR spectra of *Rhazya stricta decne* extract and the *Rhazya stricta decne* mediated gold nanoparticles

Figure 7
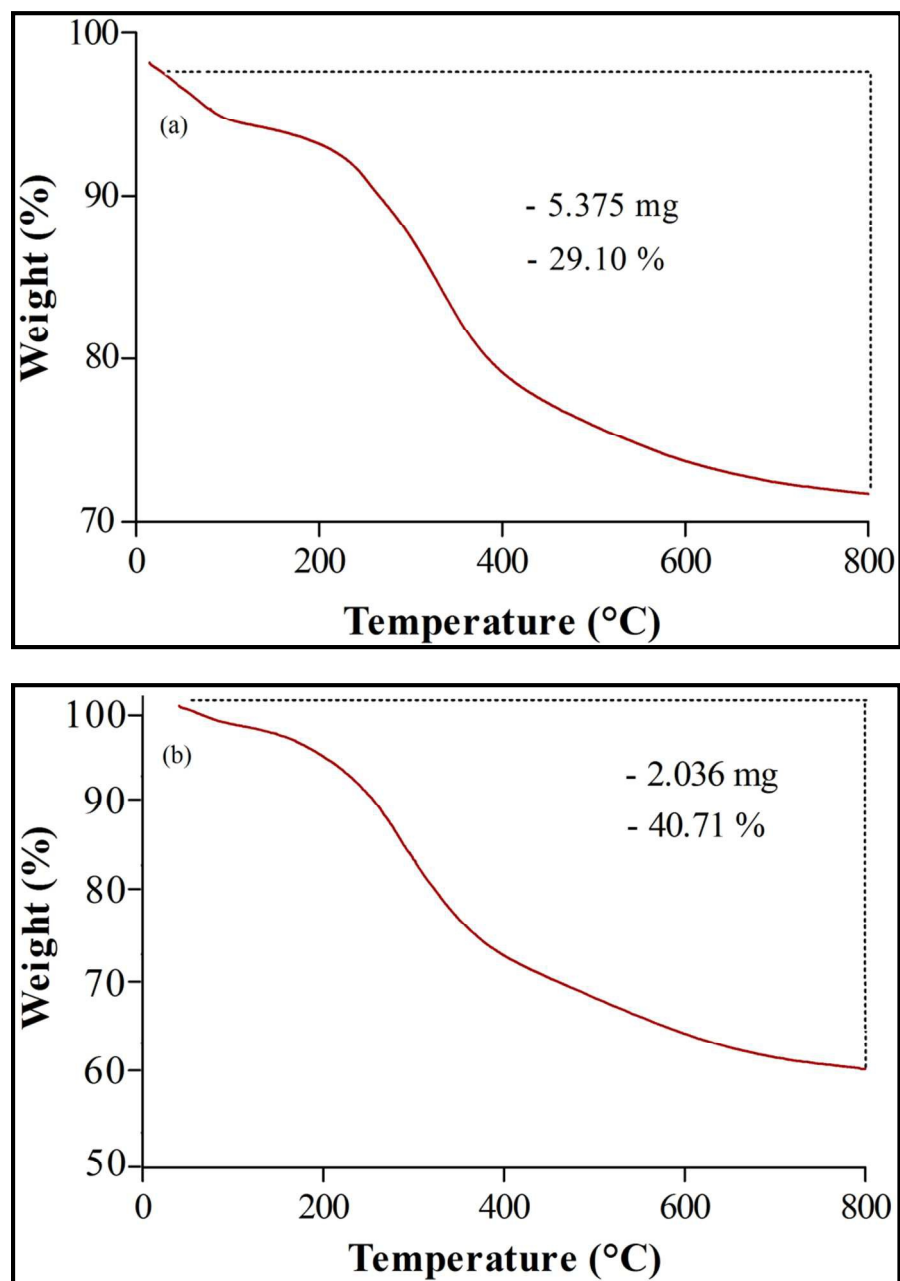
Fig. 7. Thermogravimetric analysis of AuNPs containing samples (a) gold nanoparticles from 10 and (b) 15 mL plant extract
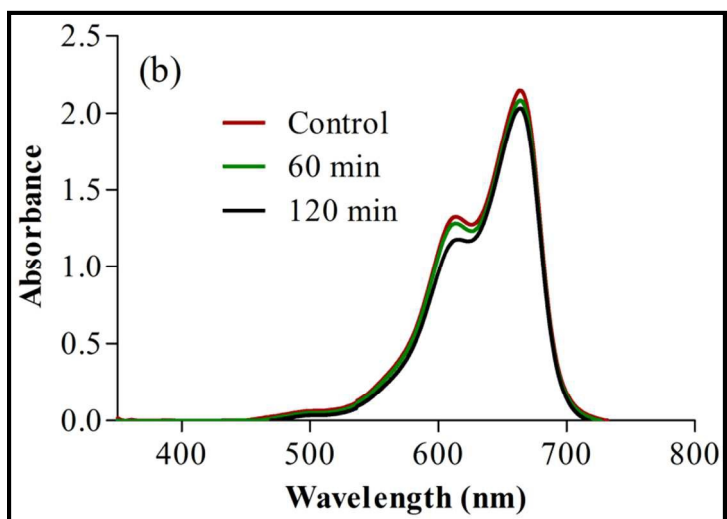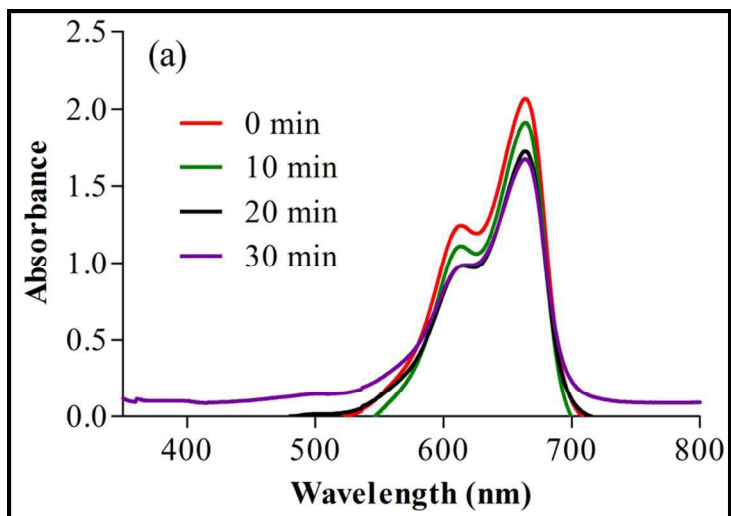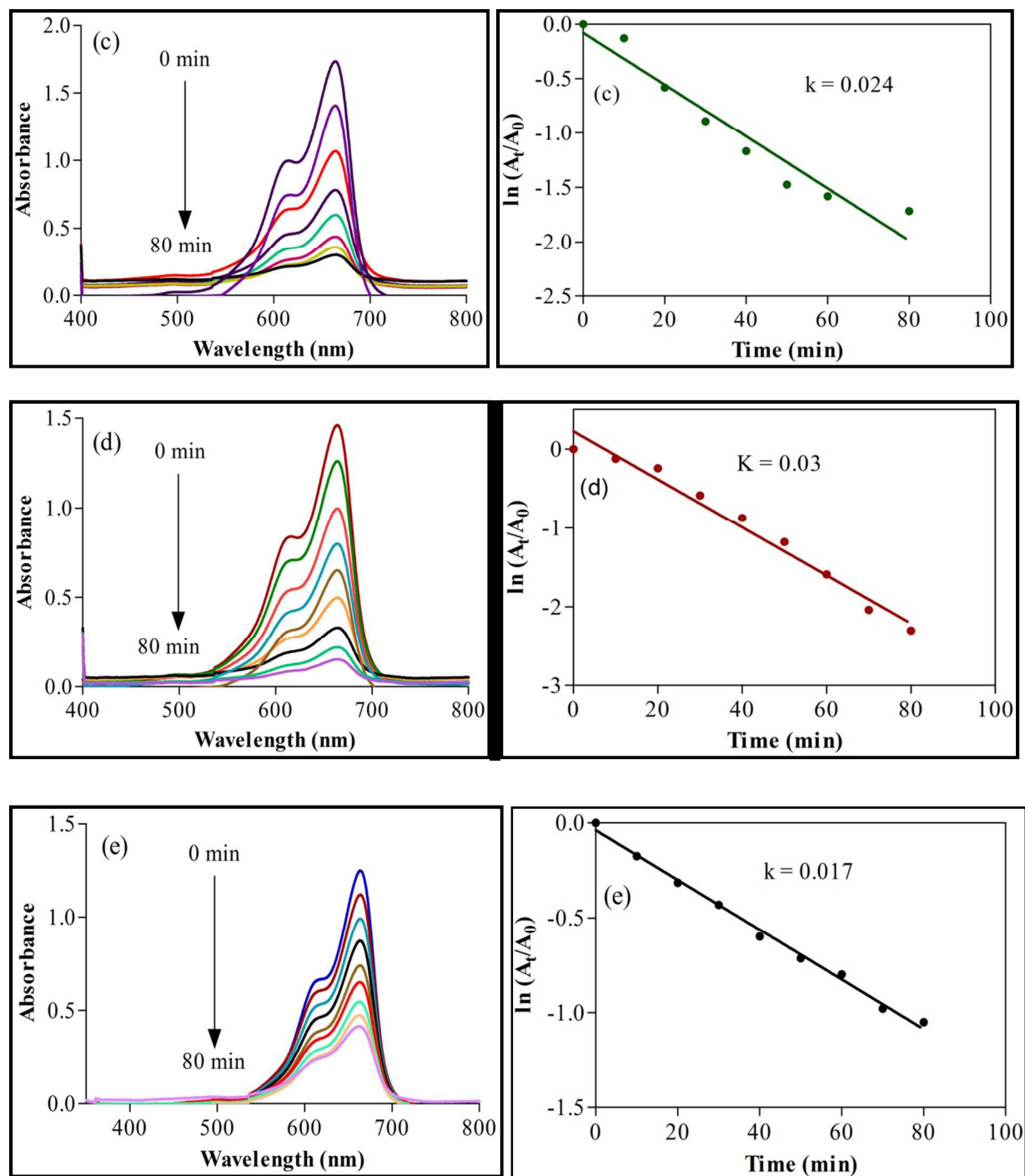
Fig. 8. UV-Vis spectra for the photocatalytic reduction of methylene blue (a) MB adsorption to nanoparticles in dark , (b) MB degradation in absence of AuNPs, (c) sample A, (d) sample B and (c) sample C (c-d) Plots of ln (A$_t$/A$_0$) versus time for the photocatalytic reduction of MB in the presence of sample A, B and C respectively

Figure 9
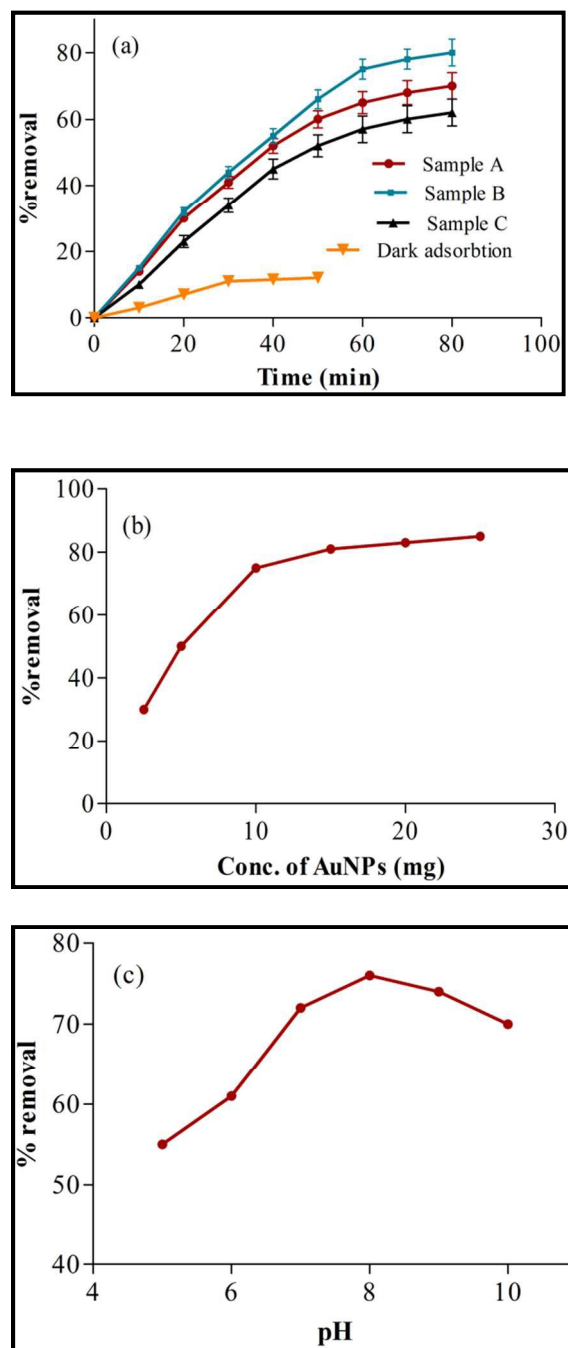
Fig. 9. (a) Photo-degradation efficiencies of methylene blue as a function of irradiation time by AuNPs of different sizes (sample A, B and C), (b) effect of catalyst amount (mg) and (c) pH

Figure 10
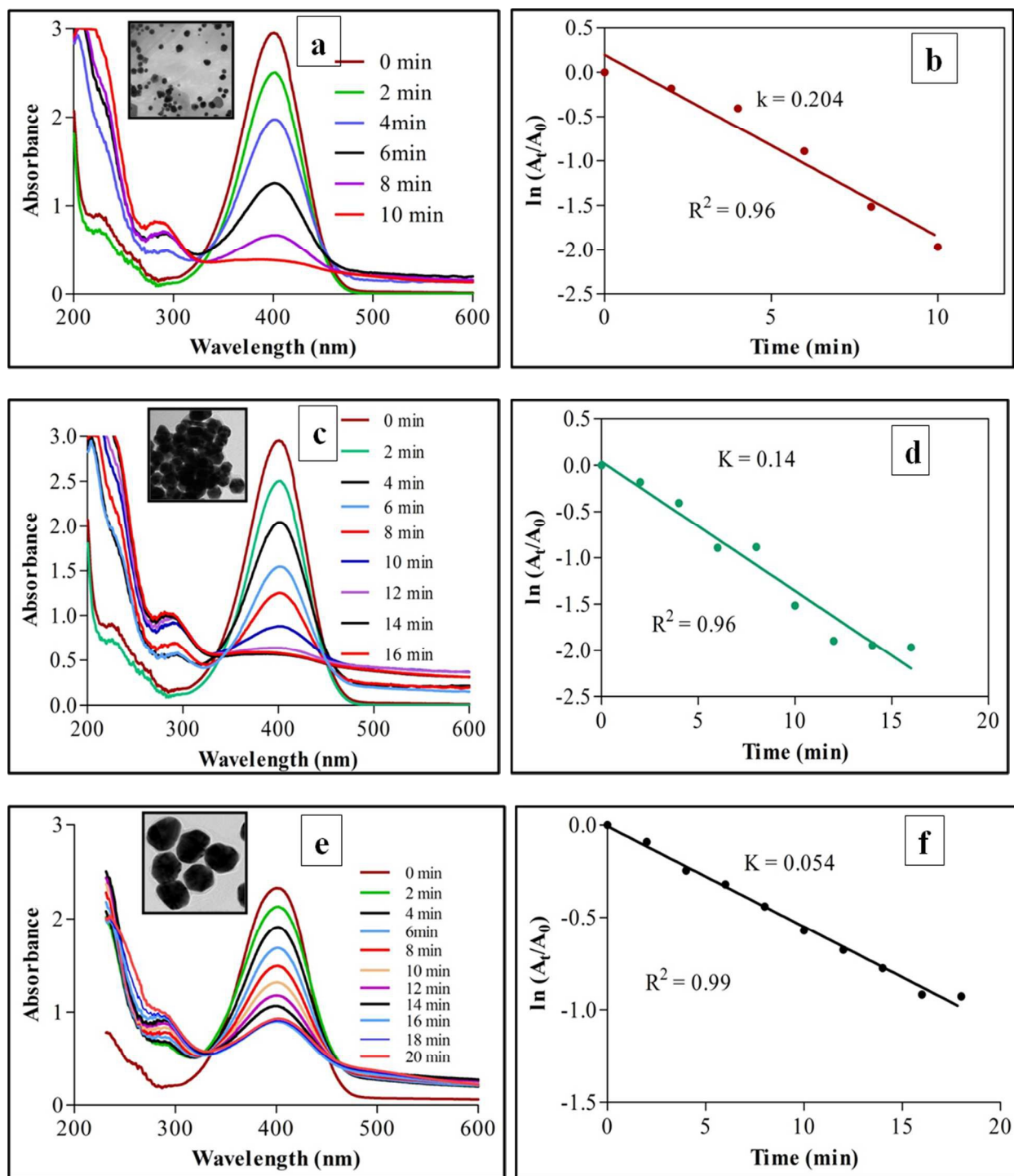
Fig. 10. UV-visible spectra for the successive reduction of 4-nitrophenol with $NaBH_4$ catalyzed by gold nanoparticles of different sizes: 20 nm (a), 50 nm (c), and 70 nm (e) and plots of ln A_t/A_0 versus time for the reduction of 4-nitrophenol using $NaBH_4$ in the presence of corresponding gold samples, inset shows the corresponding sizes of gold nanoparticles
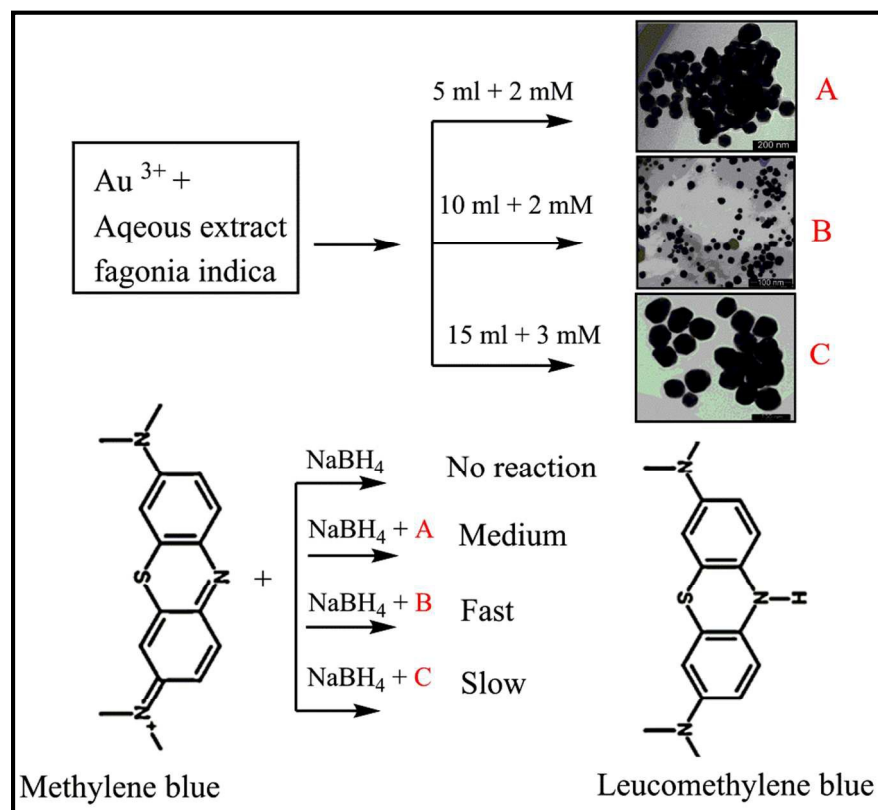
Scheme I

Scheme I. Size dependent photocatalytic degradation of methylene blue over gold nanoparticles

Scheme II
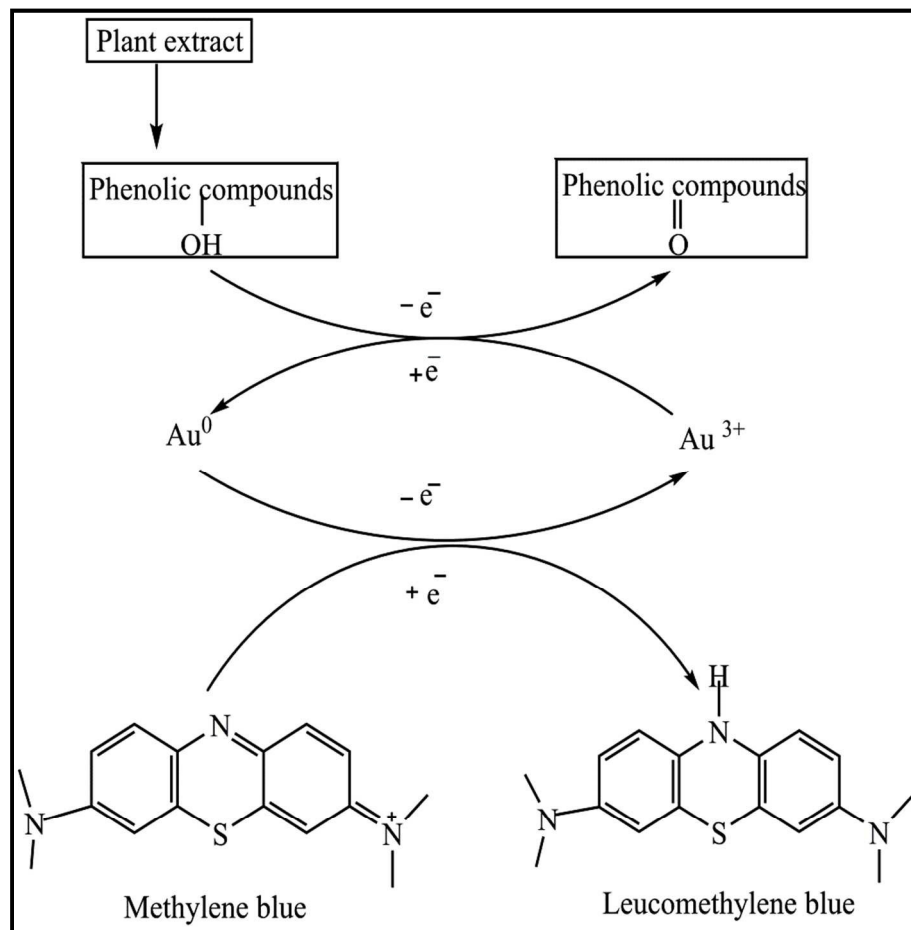
Scheme II. Gold nanoparticles act as an electron transfer mediator between donor (plant extract) and acceptor (MB) (electron relay effect).

Figure 11
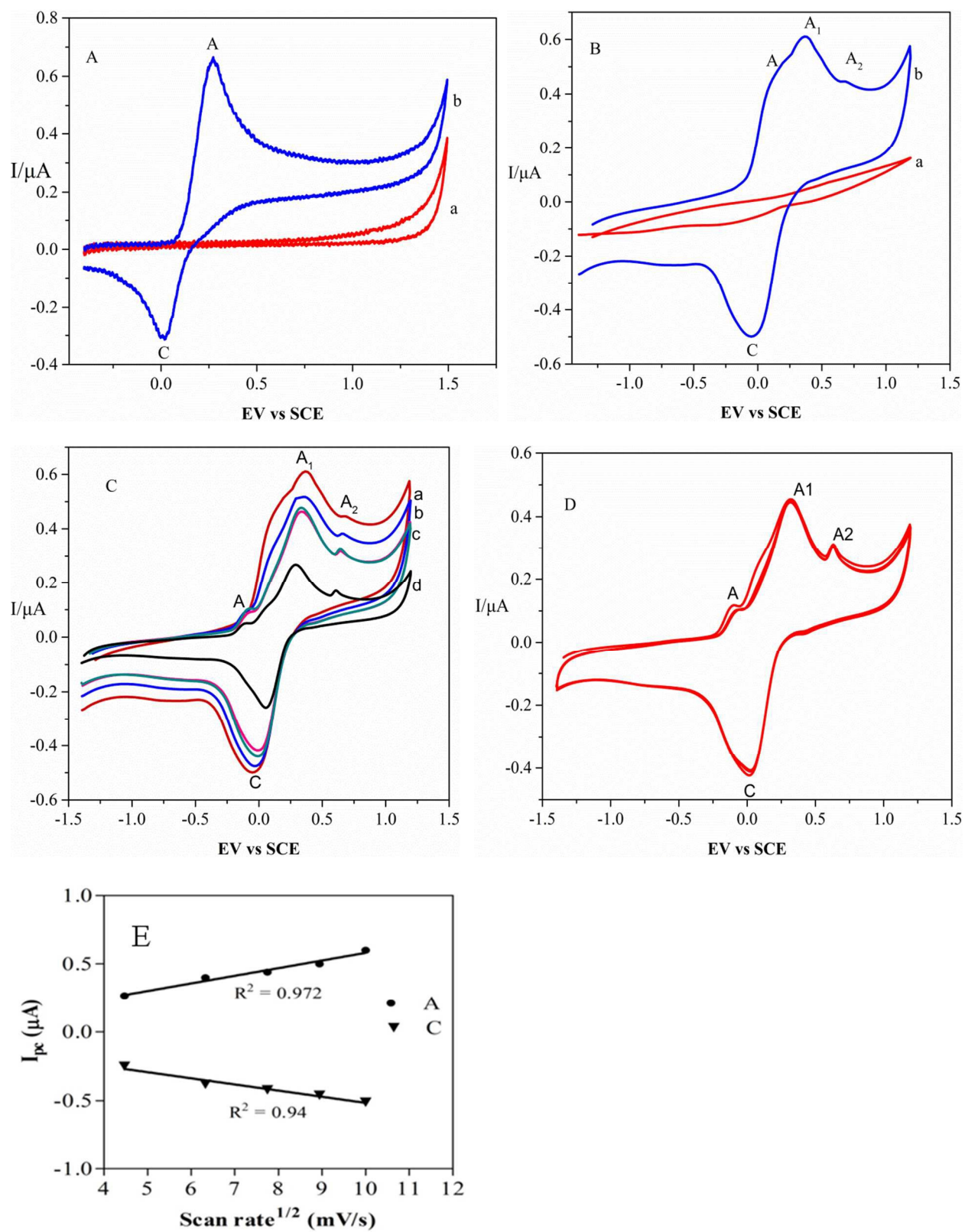
Figure 11. Cyclic voltammograms of catechol in 1.5 M sodium acetate (pH = 7) on (A) GC electrode (a) blank acetate solution (b) catechol vs SCE mV-s^{-1} at 25T (B) GC assembled AgNPs electrode in sodium acetate solution (a) blank acetate solution (b) catechol vs SCE mV-s^{-1} at 25T (C) scan rate (a)100 (b) 80 (c) 60 (d) 40 (e) 20 vs SCE mV-s^{-1} at 25T (D) multi-cyclic votammetry of catechol on GC –assemble AgNPs electrode in sodium acetate solution vs SCE mV-s^{-1} at 25T, Inset (E) calibration plot of square root of scan rate vs I$_{pa}$ and I$_{pc}$

Scheme III
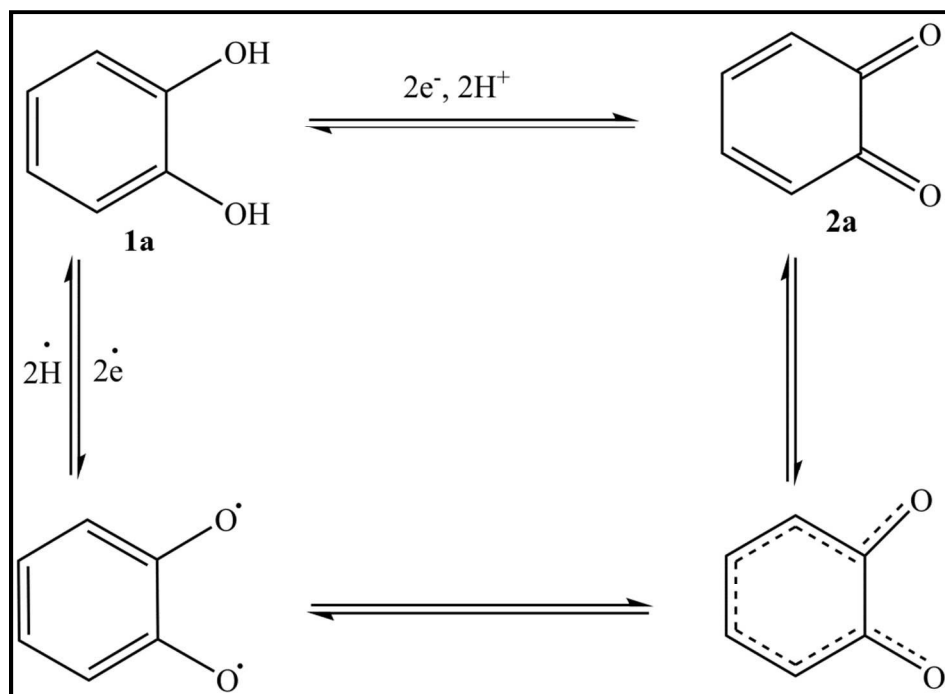
Scheme III. A reaction scheme for the multi-stepped oxidation of catechol

99x76mm (300 x 300 DPI)